Rare Met. (2024) 43(10):5410–5418
https://doi.org/10.1007/s12598-024-02802-w

RARE METALS

LETTER

A new study on formation mechanism of ordered porous anodized metal oxides

Xi-Di Sun, Xin Guo, Jia-Han Zhang, Jing Wu, Yi Shi, Hui-Yuan Sun*, Cao-Feng Pan*, Li-Jia Pan*

Received: 18 October 2023 / Revised: 31 January 2024 / Accepted: 6 February 2024 / Published online: 10 June 2024

The preparation of ordered porous metal oxide films by anodic oxidation is an efficient and simple preparation method. However, there has been no unified explanation about the formation mechanism of the porous structure for many years. In this paper, the relationship between the crystal structure of metals and the morphology of ordered porous metal oxide films is proposed. The influence of the crystal structures of different metals on the optimal morphology of porous films is discussed. Systematic studies show that anodic metals with face-centered cubic structure form highly ordered porous metal oxide films after anodic oxidation; metals with hexagonal dense arrangement form ordered nanotube arrays after anodic oxidation, but those with body-centered cubic structure form poorly ordered porous films after anodic oxidation. These results provide a new perspective and theoretical framework for the preparation of ordered porous metal oxide films by anodic oxidation.

Supplementary Information The online version contains supplementary material available at https://doi.org/10.1007/s12598-024-02802-w.

X.-D. Sun, X. Guo, J.-H. Zhang, J. Wu, Y. Shi, L.-J. Pan*
Collaborative Innovation Center of Advanced Microstructures, School of Electronic Science and Engineering, Nanjing University, Nanjing 210093, China
e-mail: ljpan@nju.edu.cn

H.-Y. Sun*
College of Physics and Hebei Advanced Thin Film Laboratory, Hebei Normal University, Shijiazhuang 050024, China
e-mail: huiyuansun@126.com

C.-F. Pan*
Institute of Atomic Manufacturing, Beihang University, Beijing 100191, China
e-mail: pancaofeng@buaa.edu.cn

Ordered porous metal oxide thin films (PMOTF) have attracted much attention due to their unique microstructural, magnetic, optical and electrical properties [1–5]. Electrochemical anodization is a simple and highly efficient preparation method that is now widely used in a number of fields [6–12]. Porous anodic alumina (PAA) membrane, in particular, is often used as a self-organized template in the field of nanomaterials [13–20] or as a substrate to prepare nanoporous materials by sputtering [21–23] because of its highly ordered nanoscale pore structural surface. The anodic growth of tantalum oxide films has received important interest due to their specific properties such as high dielectric strength, or as protective coating for surgical instruments and chemical equipment. Niobium and its oxide have been used as implant materials, biocompatible coating, and alloying element [24–28]. In recent years, titanium dioxide nanotube arrays prepared by anodic oxidation have been widely used due to their high specific surface area, unique structure and unidirectional charge transfer [29–32]. In addition, compared with the dense metal oxide films, the ordered porous metal oxide thin films itself have many excellent properties, which can be used in room temperature ferromagnetic materials, nano-energy [33], optics [34–40], sensors [41], anti-counterfeiting [42–44], and data storage [21–23, 45] fields.

Much progress has been made on the formation mechanism of the PMOTF, and theories have been provided on the synthesis of PAA [46–57], such as field-assisted dissolution (FAD) [47] and the critical current density model [50]. In recent years, a new model of the oxygen bubble mold effect (OBME) has been proposed (Fig. S1) [58–61]. Zhu et al. suggest that during the production of PMOTF, oxygen bubbles are formed at the bottom of the barrier layer. Under the action of electric field, the barrier layer

which blocks the oxygen bubbles grows upwards and finally forms a porous layer. Currently, this model can reasonably explain the formation of porous structures; however, it is still a question about what kind of pore distribution different metal metals will exhibit after anodizing. For example, the optimal morphology after anodization of alumina can show a hexagonal close-packed (hcp) ordered porous film structure [40, 53]. However, many metals such as Fe, Nb, Ta, Sn and W form porous/tubular structures after anodization [10, 30, 32, 62–65], but achieving the optimal surface morphology is difficult to form a highly ordered porous structure, while Ti, Zr and Hf metals show tubular rather than porous film structures after anodization [29, 31, 66–68].

Herein the distribution of holes after anodization of different kinds of metals is studied, and the above phenomenon is explained in combination with the OBME model. It can be found that the lattice structure of a metal determines its optimal pore distribution after anodizing, as shown in Table 1 [13–18, 21–23, 29, 31, 46–57, 66–83]. For simple lattice metals with face-centered cubic (fcc) structure, the pore distribution can form highly ordered nanopore arrays. For complex lattice metals with hcp structure, an ordered array of nanotubes is formed. However, for metals with body-centered cubic (bcc) structure, the optimal morphology of anodizing also makes it difficult to form ordered porous films. This work will provide inspiration and guidance for the preparation of porous metal oxides.

As known to all, the porous structure produced in the anodic oxidation process has a great relationship with the type of electrolyte, concentration, voltage, temperature and so on (Section SA) [84, 85]. In order to investigate the influence of the crystal structure of anode metal on the morphology of porous metal oxides, several kinds of metal with different crystal structure were selected for anodic oxidation. To obtain optimal samples, the method of two-step anodization was used. Detailed anodic oxidation parameters for each kind of metal and the morphologies of anodic oxides are listed in Table 2.

According to the OBME model, during the production process of PMOTF, miniature oxygen bubbles are first formed at the bottom of the barrier layer, and then the barrier layer blocking the oxygen bubbles grows upwards under the action of the electric field, and finally a porous layer is formed. Due to the presence of OBMs, the migration direction of anions and cations is restricted, so the original complete blocking layer map is split into independent upward-growing unit maps by each OBM, as shown in Fig. 1. An examination revealed that the morphology of nanomaterials, which was prepared by the method of template-based electrochemical deposition, exhibited a correlation with the crystalline structure of the metal [7] (Section SB). Similarly, it can be found that the optimal morphology of porous oxide films formed after anodic oxidation of metals with different crystal structures is also related to their crystal structures. This phenomenon can be explained with the OBME theory.

Al is the representative metal for the fcc structure. The detailed procedures of highly ordered porous anodic alumina (PAA) films are similar to those in references [12, 24] (Section SC). Figure 2a demonstrates the cross section of PAA, from which it can be seen that the pore size is uniform and dense. Figure 2b, c shows the surface morphology of the scanning electron microscope (SEM) and the scanning probe microscope (SPM) of PAA, respectively, from which it can be seen that the nanopore arrays on the surface of our prepared PAA films are in an ordered hexagonal close-packed pattern and are highly homogeneous.

According to the OBME model, the formation of the porous structure of anodized metal oxides results from the generation of oxygen bubbles [46–49]. In fact, the generation and distribution of oxygen bubbles are naturally related to the structure of the metal itself and the applied

Table 1 Morphology and ordering of porous structure of anodic oxides

Crystal structure	Method	Metal oxide	Pore distribution	Ordered/disordered
Al (fcc) [13–18, 21–23, 42–53, 71–75]	Anodic oxidation	Al_2O_3	Nanopore	Ordered
Ti (hcp) [64–66, 76–79]	Anodic oxidation	TiO_2	Nanotube	Ordered
Zr (hcp) [66, 67, 80–83]	Anodic oxidation	ZrO_2	Nanotube	Ordered
Hf (hcp) [68, 84]	Anodic oxidation	HfO_2	Nanotube	Ordered
Fe (bcc) [85–87]	Anodic oxidation	Ta_2O_5	Nanopore/tube	Disordered
Ta (bcc) [53, 88]	Anodic oxidation	Fe_2O_3	Nanopore/tube	Disordered
Nb (bcc) [89, 90]	Anodic oxidation	Nb_2O_5	Nanopore/tube	Disordered

Table 2 Anodic oxidation parameters and morphologies of anodic oxides

Metal (crystal structure)	Electrolyte	Potential / V	Morphology of porous anode oxides
Al (fcc)	0.3 mol·L^{-1} $H_2C_2O_4$	45	Ordered nanopore array
Ti (hcp)	Ethylene glycol containing 0.5 wt% NH_4F and 4 vol% deionized water	60	Nanotubes
Zr (hcp)	Glycerol containing 0.35 mol·L^{-1} NH_4F and 4 vol% deionized water	50	Nanotubes
Hf (hcp)	Ethylene glycol containing 0.1 mol·L^{-1} NH_4F and 1 mol·L^{-1} deionized water	40	Nanotubes
Fe (bcc)	Ethylene glycol containing 0.1 mol·L^{-1} NH_4F and 1 mol·L^{-1} deionized water	40	Disordered nanopore array
Nb (bcc)	1 mol·L^{-1} H_3PO_4 and 1.5 wt% NH_4F	15	Disordered nanopore array
Ta (bcc)	1 mol·L^{-1} H_2SO_4; 3 wt% NH_4F	35	Disordered nanopore array

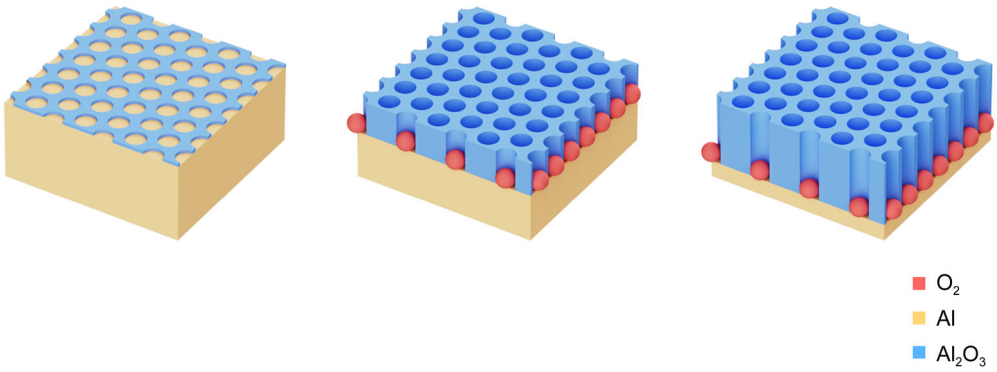

Fig. 1 Schematic diagram of oxygen bubble mold effect causing material to form a porous structure

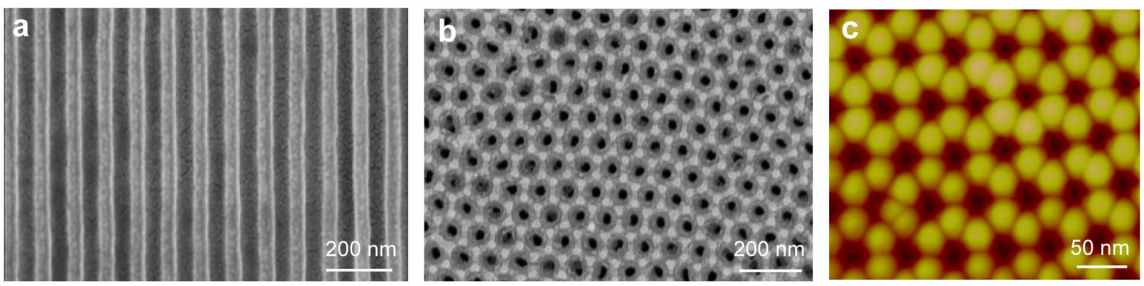

Fig. 2 **a, b** SEM cross-sectional image and surface image of PAA; **c** SPM surface image of PAA

voltage in the process of electrochemical oxidation (Fig. S2). It is known that the range of the oxidation voltage required to form the PAA film is relatively large, and the pore size of the film is also changed accordingly (Fig. S3). The higher the oxidation voltage the more significant the kinetic factors will be when using the same electrolyte, and thus the larger the pore size will form (Table S1). To obtain PAA film in sulfuric acid and oxalic acid electrolytes, a low oxidation voltage (less than 60 V) is needed. At low oxidation voltage, the reduced metal particles are easy to move onto the solid surface due to the dominant thermodynamic factors, which results in an orderly close-packing pattern of "OBM" to keep the energy minimum. Thus, the PAA grown in accordance with the OBME also shows a uniform and close-packing accumulation of holes.

PAA (H_2SO_4, $H_2C_2O_4$) was prepared using different electrolytes. At low voltages, the nanopore arrays on the PAA surface showed ordered hcp nanopores (Fig. S4a, b), due to the thermodynamic dominance, where the crystal structure of the metal plays a role. However, obtaining PAA in sulfuric acid electrolyte usually requires higher oxidation voltages (greater than 80 V). Therefore, kinetic factors dominate, resulting in irregular pore sizes and

arrangements of PAA films. In addition, the more pronounced the kinetic factors are, the larger the diameters of the oxygen bubbles become. This means that as the oxidation voltage increases, the diameter of the pores also increases. Therefore, dense and ordered PAA films cannot be obtained at large voltages (Fig. S4c).

However, for the metal with fcc structure, oxygen bubbles produced in the process of electrochemical reaction are easy to arrange in the close-packing accumulation mode under appropriate voltage due to its own close-packing accumulation structure. According to the OBME model, an ordered porous film with the holes of which are approximately equal and uniform naturally are formed (Fig. S5). Some special phenomena (nanotubes) occur in PAA films under special conditions, for example, the pores of anodic aluminum oxide (AAO) under high voltage or H_2SO_4 electrolyte will show an irregular or tubular morphology. However, the focus of this paper is solely on the impact of metal crystal structure on the optimal morphology of porous anodic oxides. These special phenomena further prove the point of this paper, which are discussed in detail in the supporting information (Section SD).

The commonly used metals for hcp structures are titanium, hafnium and zirconium, so we performed anodizing experiments with each of these three metals as samples (Section SE). As can be seen in Fig. 3a, c, e, the nanopore arrays distributed on the surface of the anodized TiO_2, HfO_2 and ZrO_2 films are also arranged in an ordered hcp pattern, which seems to be similar to that of the PAA films. However, it is clear from the SEM cross sections in Fig. 3b, d, f that highly ordered arrangements of nanotubes are inside the samples, which are quite different from the nanopore structure found within PAA films.

It is well known that the hcp structure belongs to a complex lattice structure, which is composed of two interpenetrating simple hexagonal lattices (Fig. 4a). As can be seen from Fig. 4b, along the c-axis, the lattice points are displaced from one another by a distance $c/2$ and are horizontally arranged. Figure 4c shows the stereoscopic distribution of atoms in the hcp structural metals visually. Clearly, the points of one lie directly above the centers of the triangles formed by the points of the other.

The whole hcp structure lattice can also be considered to be composed of two sets of sublattices, which translate a distance in some specific direction. In the process electrochemical reaction, it is different for the two sets of sublattices to obtain electric field effect. As a result, the sublattices with a larger electric field will be preferentially anodized. According to the oxygen bubble mold, an orderly close-packing holes distributed membrane can be formed. At the same time, a similar anodizing process occurs in another set of sublattices under a smaller electric field. There is a dislocation between the two sets of sublattices, which causes the porous structure formed by the two sets of sublattices to separate at the closest point inside, and a tubular structure is produced in the end. That is to say, the tubular structure obtained by anodizing the metal of the hcp structure is obtained through two sets of the porous structure formed by two sets of sublattices. Moreover, the two sets of porous structures grow are not synchronized, and so the lengths of the tubes corresponding to the two sets of sublattices should also be different (Fig. S6a). Also, a similar result was obtained by Zhang et al., with a 0.02 μm difference in the length of the TiO_2 nanotubes, which further confirms our inference [24]. SEM surface topography of porous TiO_2 similarly demonstrates the internal

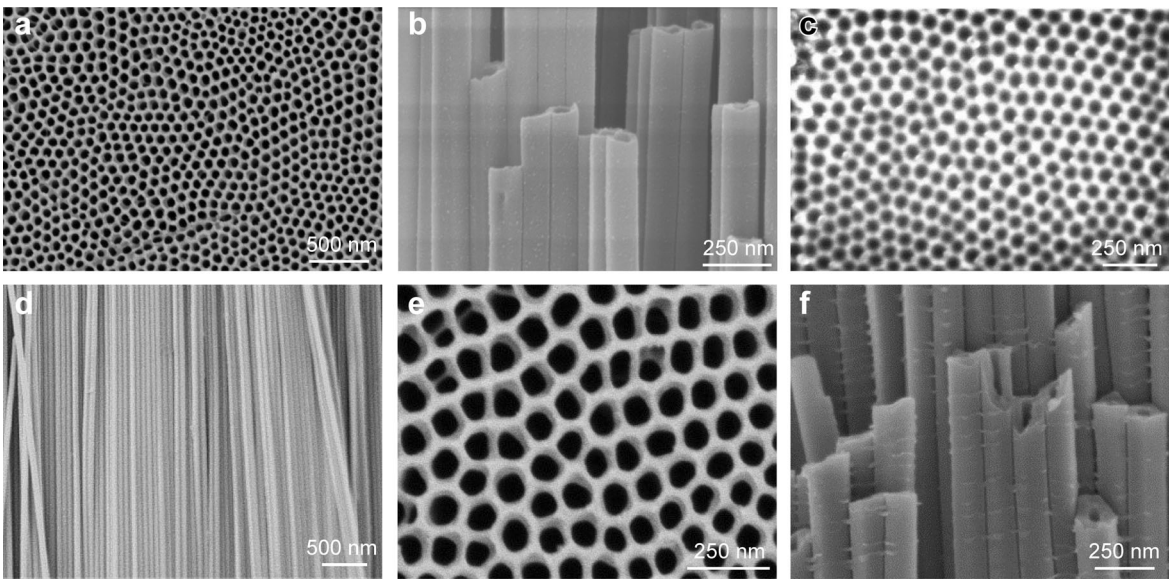

Fig. 3 SEM surface images and cross-sectional images about hcp structure: **a**, **b** TiO_2; **c**, **d** HfO_2; **e**, **f**: ZrO_2

separation of the tubular structure (Fig. S6b). Different with the complex lattice (hcp), metals with simple lattice structure can only form porous structural oxide films instead of tubular structure ones because of all the atoms are completely equivalent in them.

Similar to the above studies on hcp structure, three other metals of niobium, tantalum and iron with bcc structure were chosen for experiments and obtained similar results (Section SF). For the bcc-structured metals, the distribution of nanopore arrays in the anodized niobium, tantalum and iron films is no longer uniformly ordered. As shown in Fig. 5a, c, e, the surface of the anodized bcc-structured metal exhibits an extremely irregular and porous structure. Figure 5b, d, f shows that the interior of the anodic oxide of the bcc-structured metal exhibits a haphazard distribution of irregular holes or tubes. This is because both the fcc structure and the hcp structure belong to the close-packed arrangement of metals, while the distribution of metal ions on the (111) crystal plane of the bcc structure is similar to that of the close-packed arrangement of the fcc structure. However, the distribution of metal ions on the (100) crystal plane is similar to the ion distribution of the hcp structure, so the anodic oxide film with both porous and tubular structures can be obtained. When the metal of bcc structure with the preferred orientation of (111) plane is used, the porous structure is obtained. When the (100) plane orientation is preferred, the tubular structure is obtained (Fig. S7). When the metal ions are distributed on the (111) and (100) crystal planes of the bcc structure, it can be seen from Fig. S8 that the lattice point distribution can be approximated as two sets of simple cubic sublattices when the plane direction is [100], while it can be regarded as a dense stacking arrangement when the plane direction is (111). If there is no preferred orientation, the holes and tubes are mixed, making the inside of the anodized film very irregular. Although the metal with bcc structure can

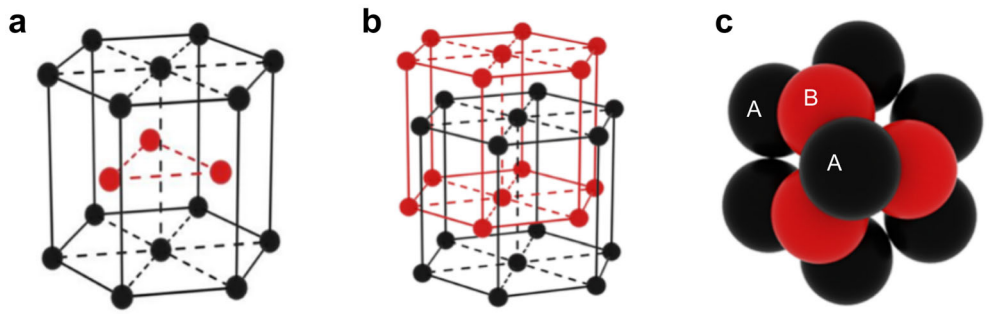

Fig. 4 Schematic representation of hcp crystal structure

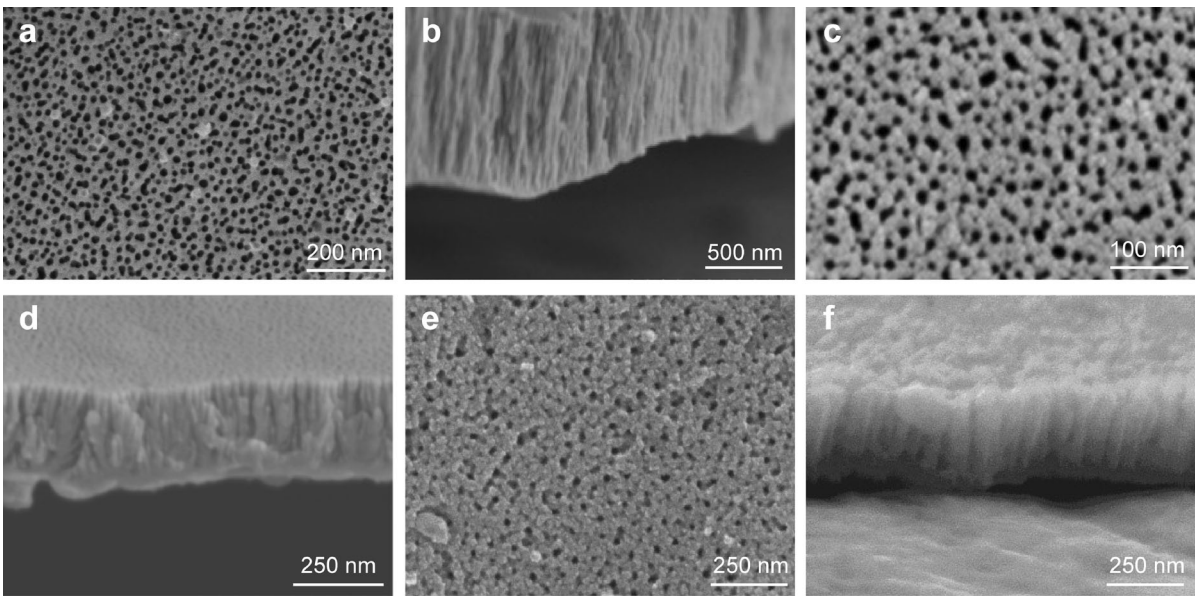

Fig. 5 SEM surface images and cross-sectional images about bcc structure: **a**, **b** Nb_2O_5; **c**, **d** Ta_2O_5; **e**, **f** Fe_2O_3

form both porous and tubular films, the metal atoms cannot form evenly spaced close-packed accumulation, the corresponding oxygen bubbles naturally vary in size, which leads to varying sizes of porous or tubes and poor order. For example, when the (001) oriented bcc metal is used, an ordered porous structure may also be obtained after anodic oxidation. However, further research is needed on this issue.

From the experimental results described above, it is found that the morphology of porous metal oxide film prepared by anodic oxidation is closely related to the crystalline structure of the metals. For fcc structure metals, the highly ordered nanoporous film will be formed after anodic oxidation, and the nanopore arrays in the surface of the film are arranged in an orderly hcp pattern. For hcp structure metals, a thin film constituted of nanotubes after anodic oxidation. For bcc structure metals, however, a disordered porous film is formed after anodizing. It is interesting in finding that simple lattice structure and complex lattice structure determine the formation of nanopores and nanotubes in anodic oxides. And whether the crystal structure is close-packed or not determines the ordered/disordered nature of the formed nanopores. Specifically, after anodic oxidation, simple lattice metals and complex lattice metals have different internal structures. Metals with simple lattice structures (fcc and bcc) are anodized to form a nanoporous structure film. The metal with a composite lattice structure (hcp) is anodized to form a nanotube structure film.

From the above discussion, it can be inferred that the morphology of the porous anode oxide is related to the structure of the anode metal. This is mainly due to the distribution of oxygen bubbles related to the crystal structure of the anode metal. Therefore, it is not difficult to understand that the morphology of the corresponding oxides may change for specially treated metals or metals grown in different orientations. This is especially true when these orientation-grown metals are used for anodizing. Although the morphology that emerges after anodizing does not correspond to our proposed morphology, these metals still demonstrate the influence of the crystal structure on the surface morphology of the anodic oxides.

In summary, it is found that the morphology of the porous anode oxide is related to the structure of the anode metal. For metal materials with close-packed crystalline structures (fcc and hcp), an ordered porous distribution pattern will be formed by anodizing. For simple lattice metals (such as aluminum) with fcc structure, the distribution of holes is a highly ordered nanoporous array. While for complex lattice metals (such as titanium, zirconium, hafnium) with hcp structure, the ordered nanotubes arrays are formed by anodic oxidation. The unique tubular structure may be caused by the distribution of oxygen bubbles produced by anodic oxidation, which is related to the crystal structure. It is noted that, for simple lattice metals (such as iron, niobium and tantalum) with bcc structure, although porous or tubes films are also formed after anodizing, they are usually irregular. In conclusion, the formation of porous metal oxides is essentially the result of a combination of crystal structure and thermodynamic and kinetic factors.

Acknowledgements This work was financially supported by the National Key Research and Development program of China (Nos. 2021YFA1401103 and 2016YFA0202703), the National Natural Science Foundation of China (Nos. 61825403, 61921005 and 61674078), the Natural Science Foundation of Hebei Province (No. A2020205038) and the Postgraduate Demonstration Course Project of Hebei Province (No. KCJSX2021038).

Declarations

Conflict of interests The authors declare that they have no conflict of interest.

References

[1] Chen XY, Wang XZ, Liu FJ, Zhang GS, Song XJ, Tian J, Cui HZ. Fabrication of porous Zn_2TiO_4–ZnO microtubes and analysis of their acetone gas sensing properties. Rare Met. 2021; 40(6):1528. https://doi.org/10.1007/s12598-020-01518-x.

[2] Sun XD, Yu HW, Zhao CY, Zhang J, Shi Y, Pan LJ. Tunable structural coloration of ultrathin zirconia nanotubes film. Rare Met. 2023;42(10):3304. https://doi.org/10.1007/s12598-023-02313-0.

[3] Zheng QY, Yang M, Dong X, Zhang XF, Cheng XL, Huo LH, Major Z, Xu YM. ZnO/PANI nanoflake arrays sensor for ultra-low concentration and rapid detection of NO at room temperature. Rare Met. 2023;42(2):536. https://doi.org/10.1007/s12598-022-02149-0.

[4] Gao WX, Chang XT, Zhu XJ, Li JF, Jiang YC, Wang DS, Yang CX, Sun SB. Al-doped ZnO/WO heterostructure films prepared by magnetron sputtering for isopropanol sensors. Rare Met. 2023. https://doi.org/10.1007/s12598-023-02406-w.

[5] Ding QW, Luo Q, Lin L, Fu XP, Wang LS, Yue GH, Lin J, Xie QS, Peng DL. Facile synthesis of PdCu nanocluster-assembled granular films as highly efficient electrocatalysts for formic acid oxidation. Rare Met. 2022;41(8):2595. https://doi.org/10.1007/s12598-022-01997-0.

[6] Zaffora A, Cho DY, Lee KS, Di Quarto F, Waser R, Santamaria M, Valov I. Electrochemical tantalum oxide for resistive switching memories. Adv Mater. 2017;29(43):6. https://doi.org/10.1002/adma.201703357.

[7] Gombar M, Vagaska A, Harnicarova M, Valicek J, Kusnerova M, Czan A, Kmec J. Experimental analysis of the influence of factors acting on the layer thickness formed by anodic oxidation of aluminium. Coatings. 2019;9(1):21. https://doi.org/10.3390/coatings9010057.

[8] Rangaraju RR, Raja KS, Panday A, Misra M. An investigation on room temperature synthesis of vertically oriented arrays of iron oxide nanotubes by anodization of iron. Electrochim Acta. 2010;55(3):785. https://doi.org/10.1016/j.electacta.2009.07.012.

[9] Choi YW, Shin S, Park DW, Choi J. Surface treatment of iron by electrochemical oxidation and subsequent annealing for the

improvement of anti-corrosive properties. Curr Appl Phys. 2014;14(5):641. https://doi.org/10.1016/j.cap.2014.02.014.
[10] Cong ZZ, Wang ML, Sun XD, Liu LH, Sun HY. Optical and dielectric properties of anodic iron oxide films. Appl Surf Sci. 2020;503:7. https://doi.org/10.1016/j.apsusc.2019.144159.
[11] Zhang MM, Chen JY, Li H, Wang CR. Recent progress in Li-ion batteries with TiO2 nanotube anodes grown by electrochemical anodization. Rare Met. 2021;40(2):249. https://doi.org/10.1007/s12598-020-01499-x.
[12] Wu T, Sun MZ, Huang BL. Non-noble metal-based bifunctional electrocatalysts for hydrogen production. Rare Met. 2022;41(7):2169. https://doi.org/10.1007/s12598-021-01914-x.
[13] Zhang XL, Zhang HM, Wu TS, Li ZY, Zhang ZJ, Sun HY. Comparative study in fabrication and magnetic properties of FeNi alloy nanowires and nanotubes. J Magn Magn Mater. 2013;331:162. https://doi.org/10.1016/j.jmmm.2012.11.033.
[14] Zhang HM, Zhang XL, Zhang JJ, Li ZY, Sun HY. Template-based electrodeposition growth mechanism of metal nanotubes. J Electrochem Soc. 2013;160(2):D41. https://doi.org/10.1149/2.049302jes.
[15] Zhang HM, Zhang XL, Wu TS, Zhang ZJ, Zheng JF, Sun HY. Template-based synthesis and discontinuous hysteresis loops of cobalt nanotube arrays. J Mater Sci. 2013;48(21):7392. https://doi.org/10.1007/s10853-013-7554-8.
[16] Sousa CT, Leitao DC, Proenca MP, Ventura J, Pereira AM, Araujo JP. Nanoporous alumina as templates for multifunctional applications. Appl Phys Rev. 2014;1(3):22. https://doi.org/10.1063/1.4893546.
[17] Dryden DM, Vidu R, Stroeve P. Nanowire formation is preceded by nanotube growth in templated electrodeposition of cobalt hybrid nanostructures. Nanotechnology. 2016;27(44):8. https://doi.org/10.1088/0957-4484/27/44/445302.
[18] Jeon YS, Kim SH, Park BC, Nam DY, Kim YK. Synthesis of Co nanotubes by nanoporous template-assisted electrodeposition via the incorporation of vanadyl ions. Chem Commun. 2017;53(11):1825. https://doi.org/10.1039/c6cc09843f.
[19] Cui J, Wang H, Sun DL, Zhang QA, Zhu M. Realizing nano-confinement of magnesium for hydrogen storage using vapour transport deposition. Rare Met. 2016;35(5):401. https://doi.org/10.1007/s12598-014-0272-9.
[20] Wang M, Zhang S, Du ZF, Sun LD, Zhao DL. Novel dye-sensitized solar cell architecture using TiO2-coated Ag nanowires array as photoanode. Rare Met. 2019;38(4):316. https://doi.org/10.1007/s12598-014-0433-x.
[21] Sun XD, Mo XM, Liu LH, Sun HY, Pan CF. Voltage-driven room-temperature resistance and magnetization switching in ceramic TiO_2/PAA nanoporous composite films. ACS Appl Mater Interfaces. 2019;11(24):21661. https://doi.org/10.1021/acsami.9b02593.
[22] Qi LQ, Liu HY, Sun HY, Liu LH, Han RS. Electric field control of magnetization in Cu_2O/porous anodic alumina hybrid structures at room temperature. Appl Phys Lett. 2016;108(14):4. https://doi.org/10.1063/1.4945602.
[23] Qi LQ, Pan DY, Li JQ, Liu LH, Sun HY. HfO_2/porous anodic alumina composite films for multifunctional data storage media materials under electric field control. Nanotechnology. 2017;28(11):7. https://doi.org/10.1088/1361-6528/aa5a5c.
[24] Sun HY, Zhang HM, Hou X, Liu LH, Wu TS, Yang SM. Significant room temperature ferromagnetism in PAA thin films. J Mater Chem C. 2013;1(22):3569. https://doi.org/10.1039/c3tc30462k.
[25] Esmaeily AS, Venkatesan M, Sen S, Coey JMD. D-zero magnetism in nanoporous amorphous alumina membranes. Phys Rev Mater. 2018;2(5):12. https://doi.org/10.1103/PhysRevMaterials.2.054405.
[26] Yang K, Yang K, Bao YF, Jiang YF. Formation mechanism of titanium and niobium carbides in hardfacing alloy. Rare Met. 2017;36(8):640. https://doi.org/10.1007/s12598-016-0777-5.
[27] Li GZ, Tang HP, Zhang WY, Li G, Yu LL, Li YN. Fabrication of multilayer Nb2O5 nanoporous film by anodization of niobium foils. Rare Met. 2015;34(2):77. https://doi.org/10.1007/s12598-013-0140-z.
[28] Lu LW, Luo H, Li GX, Li Y, Wang XH, Huang CK, Lan ZQ, Zhou WZ, Guo J, Ismail M, Liu HZ. Layered niobium carbide enabling excellent kinetics and cycling stability of Li-Mg-B-H hydrogen storage material. Rare Met. 2023. https://doi.org/10.1007/s12598-023-02489-5.
[29] Zhang YL, Yu DL, Gao MQ, Li DD, Song Y, Jin R, Ma WH, Zhu XF. Growth of anodic TiO_2 nanotubes in mixed electrolytes and novel method to extend nanotube diameter. Electrochim Acta. 2015;160:33. https://doi.org/10.1016/j.electacta.2015.02.058.
[30] Tsuchiya H, Macak JM, Sieber I, Taveira L, Ghicov A, Sirotna K, Schmuki P. Self-organized porous WO_3 formed in NaF electrolytes. Electrochem Commun. 2005;7(3):295. https://doi.org/10.1016/j.elecom.2005.01.003.
[31] Regonini D, Bowen CR, Jaroenworaluck A, Stevens R. A review of growth mechanism, structure and crystallinity of anodized TiO2 nanotubes. Mater Sci Eng R-Rep. 2013;74(12):377. https://doi.org/10.1016/j.mser.2013.10.001.
[32] Li PY, Niu DM, He MF, Huang H, Ying ZR, Xu HQ, Zhu JW, Zhu XF. Growth model of the tin anodizing process and the capacitive, performance of porous tin oxides. J Phys Chem C. 2020;124(5):3050. https://doi.org/10.1021/acs.jpcc.9b09648.
[33] Lee J, Kim D, Choi CH, Chung W. Nanoporous anodic alumina oxide layer and its sealing for the enhancement of radiative heat dissipation of aluminum alloy. Nano Energy. 2017;31:504. https://doi.org/10.1016/j.nanoen.2016.12.007.
[34] Santos A, Yoo JH, Rohatgi CV, Kumeria T, Wang Y, Losic D. Realisation and advanced engineering of true optical rugate filters based on nanoporous anodic alumina by sinusoidal pulse anodisation. Nanoscale. 2016;8(3):1360. https://doi.org/10.1039/c5nr05462a.
[35] Kuang D, Charriere R, Matsapey N, Flury M, Faucheu J, Chavel P. Modeling the specular spectral reflectance of partially ordered alumina nanopores on an aluminum substrate. Opt Express. 2015;23(4):4506. https://doi.org/10.1364/oe.23.004506.
[36] Manzano CV, Best JP, Schwiedrzik JJ, Cantarero A, Michler J, Philippe L. The influence of thickness, interpore distance and compositional structure on the optical properties of self-ordered anodic aluminum oxide films. J Mater Chem C. 2016;4(32):7658. https://doi.org/10.1039/c6tc01904h.
[37] Chen YT, Santos A, Ho D, Wang Y, Kumeria T, Li JS, Wang CH, Losic D. On The generation of interferometric colors in high purity and technical grade aluminum: an alternative green process for metal finishing industry. Electrochim Acta. 2015;174:672. https://doi.org/10.1016/j.electacta.2015.06.066.
[38] Xu Q, Sun HY, Yang YH, Liu LH, Li ZY. Optical properties and color generation mechanism of porous anodic alumina films. Appl Surf Sci. 2011;258(5):1826. https://doi.org/10.1016/j.apsusc.2011.10.054.
[39] Xu Q, Yang YH, Gu JJ, Li ZY, Sun HY. Influence of Al substrate on the optical properties of porous anodic alumina films. Mater Lett. 2012;74:137. https://doi.org/10.1016/j.matlet.2012.01.076.
[40] Xu Q, Yang YH, Liu LH, Gu JJ, Liu JJ, Li ZY, Sun HY. Synthesis and Optical Properties of Iridescent Porous Anodic Alumina Thin Films. J Electrochem Soc. 2012;159(1):C25. https://doi.org/10.1149/2.016201jes.
[41] Bolokang AS, Cummings FR, Dhonge BP, Abdallah HMI, Moyo T, Swart HC, Arendse CJ, Muller TFG, Motaung DE. Characteristics of the mechanical milling on the room

temperature ferromagnetism and sensing properties of TiO_2 nanoparticles. Appl Surf Sci. 2015;331:362. https://doi.org/10.1016/j.apsusc.2015.01.055.
[42] Yoon B, Lee J, Park IS, Jeon S, Lee J, Kim JM. Recent functional material based approaches to prevent and detect counterfeiting. J Mater Chem C. 2013;1(13):2388. https://doi.org/10.1039/c3tc00818e.
[43] Xu Q, Ye WJ, Feng SZ, Sun HY. Synthesis and properties of iridescent Co-containing anodic aluminum oxide films. Dyes Pigment. 2014;111:185. https://doi.org/10.1016/j.dyepig.2014.06.012.
[44] Wang YL, Han RH, Qi LQ, Liu LH, Sun HY. Synthesis of ultrathin TiO_2/Ti films with tunable structural color. Appl Opt. 2016;55(35):10002. https://doi.org/10.1364/ao.55.010002.
[45] Santos A, Law CS, Pereira T, Losic D. Nanoporous hard data: optical encoding of information within nanoporous anodic alumina photonic crystals. Nanoscale. 2016;8(15):8091. https://doi.org/10.1039/c6nr01068g.
[46] Spooner RC, Forsyth WJ. X-Ray emission spectroscopic investigation of sealing of anodic oxide films on aluminium. Nature. 1963;200(491):1002. https://doi.org/10.1038/2001002a0.
[47] Sullivan JPO, Wood JC. The morphology and mechanism of formation of porous anodic films on aluminium. P Roy Soc A-Math Phy. 1970;317(1531):511. https://doi.org/10.1098/rspa.1970.0129.
[48] Thompson GE, Furneaux RC, Wood GC, Richardson JA, Goode JS. Nucleation and growth of porous anodic films on aluminum. Nature. 1978;272(5652):433. https://doi.org/10.1038/272433a0.
[49] Thompson GE, Shimizu K, Wood GC. Observation of flaws in anodic films on aluminum. Nature. 1980;286(5772):471. https://doi.org/10.1038/286471a0.
[50] Xu Y, Thompson GE, Wood GC. Mechanism of anodic film growth on aluminium. Trans IMF. 1985;63(1):98. https://doi.org/10.1080/00202967.1985.11870715.
[51] Despi A, Parkhutik VPJSU. Electrochemistry of aluminum in aqueous solutions and physics of its anodic oxide. 1989.
[52] Furneaux RC, Rigby WR, Davidson AP. The formation of controlled-porosity membranes from anodically oxidized aluminum. Nature. 1989;337(6203):147. https://doi.org/10.1038/337147a0.
[53] Masuda H, Fukuda K. Ordered metal nanohole arrays made by a 2-step replication of honeycomb structures of anodic alumina. Science. 1995;268(5216):1466. https://doi.org/10.1126/science.268.5216.1466.
[54] Thompson GE. Porous anodic alumina: fabrication, characterization and applications. Thin Solid Films. 1997;297(1–2):192. https://doi.org/10.1016/s0040-6090(96)09440-0.
[55] Masuda H, Hasegwa F, Ono S. Self-ordering of cell arrangement of anodic porous alumina formed in sulfuric acid solution. J Electrochem Soc. 1997;144(5):L127. https://doi.org/10.1149/1.1837634.
[56] Li FY, Zhang L, Metzger RM. On the growth of highly ordered pores in anodized aluminum oxide. Chem Mater. 1998;10(9):2470. https://doi.org/10.1021/cm980163a.
[57] Lee W, Ji R, Gosele U, Nielsch K. Fast fabrication of long-range ordered porous alumina membranes by hard anodization. Nat Mater. 2006;5(9):741. https://doi.org/10.1038/nmat1717.
[58] Zhu XF, Liu L, Song Y, Jia HB, Yu HD, Xiao XM, Yang XL. Oxygen bubble mould effect: serrated nanopore formation and porous alumina growth. Mon Chem. 2008;139(9):999. https://doi.org/10.1007/s00706-008-0893-5.
[59] Yu MS, Chen Y, Li C, Yan S, Cui HM, Zhu XF, Kong JS. Studies of oxide growth location on anodization of Al and Ti provide evidence against the field-assisted dissolution and field-assisted ejection theories. Electrochem Commun. 2018;87:76. https://doi.org/10.1016/j.elecom.2018.01.003.
[60] Yu MS, Li C, Yang YB, Xu SK, Zhang K, Cui HM, Zhu XF. Cavities between the double walls of nanotubes: evidence of oxygen evolution beneath an anion-contaminated layer. Electrochem Commun. 2018;90:34. https://doi.org/10.1016/j.elecom.2018.03.009.
[61] Zhang JJ, Huang WQ, Zhang K, Li DZ, Xu HQ, Zhu XF. Bamboo shoot nanotubes with diameters increasing from top to bottom: evidence against the field-assisted dissolution equilibrium theory. Electrochem Commun. 2019;100:48. https://doi.org/10.1016/j.elecom.2019.01.019.
[62] Sieber I, Hildebrand H, Friedrich A, Schmuki P. Formation of self-organized niobium porous oxide on niobium. Electrochem Commun. 2005;7(1):97. https://doi.org/10.1016/j.elecom.2004.11.012.
[63] Choi JS, Lim JH, Lee SC, Chang JH, Kim KJ, Cho MA. Porous niobium oxide films prepared by anodization in HF/H_3PO_4. Electrochim Acta. 2006;51(25):5502. https://doi.org/10.1016/j.electacta.2006.02.024.
[64] Wei W, Macak JM, Schmuki P. High aspect ratio ordered nanoporous Ta_2O_5 films by anodization of Ta. Electrochem Commun. 2008;10(3):428. https://doi.org/10.1016/j.elecom.2008.01.004.
[65] Shin HC, Dong J, Liu ML. Porous tin oxides prepared using an anodic oxidation process. Adv Mater. 2004;16(3):237. https://doi.org/10.1002/adma.200305660.
[66] Tsuchiya H, Macak JM, Ghicov A, Taveira L, Schmuki P. Self-organized porous TiO_2 and ZrO_2 produced by anodization. Corros Sci. 2005;47(12):3324. https://doi.org/10.1016/j.corsci.2005.05.041.
[67] Stepien M, Handzlik P, Fitzner K. Synthesis of ZrO_2 nanotubes in inorganic and organic electrolytes by anodic oxidation of zirconium. J Solid State Electrochem. 2014;18(11):3081. https://doi.org/10.1007/s10008-014-2422-2.
[68] Tsuchiya H, Schmuki P. Self-organized high aspect ratio porous hafnium oxide prepared by electrochemical anodization. Electrochem Commun. 2005;7(1):49. https://doi.org/10.1016/j.elecom.2004.11.004.
[69] Zhang ZH, Hossain MF, Takahashi T. Fabrication of shape-controlled alpha-Fe_2O_3 nanostructures by sonoelectrochemical anodization for visible light photocatalytic application. Mater Lett. 2010;64(3):435. https://doi.org/10.1016/j.matlet.2009.10.071.
[70] Yahalom J, Zahavi J. Electrolytic breakdown crystallization of anodic oxide films on Al, Ta and Ti. Electrochim Acta. 1970;15(9):1429. https://doi.org/10.1016/0013-4686(70)80064-0.
[71] Wierzbicka E, Syrek K, Maczka K, Sulka GD. Photocatalytic decolorization of methyl red on nanoporous anodic ZrO_2 of different crystal structures. Crystals. 2021;11(2):11. https://doi.org/10.3390/cryst11020215.
[72] Tsuchiya H, Macak JM, Sieber I, Schmuki P. Anodic porous zirconium oxide prepared in sulfuric acid electrolytes. Mater Sci Forum. 2006;512:205. https://doi.org/10.4028/www.scientific.net/MSF.512.205.
[73] Tsuchiya H, Macak JM, Sieber I, Schmuki P. Self-organized high-aspect-ratio nanoporous zirconium oxides prepared by electrochemical anodization. Small. 2005;1(7):722. https://doi.org/10.1002/smll.200400163.
[74] Sagu JS, Wijayantha KGU, Bohm M, Bohm S, Rout TK. Anodized steel electrodes for supercapacitors. ACS Appl Mater Interfaces. 2016;8(9):6277. https://doi.org/10.1021/acsami.5b12107.
[75] Roy P, Kim D, Lee K, Spiecker E, Schmuki P. TiO_2 nanotubes and their application in dye-sensitized solar cells. Nanoscale. 2010;2(1):45. https://doi.org/10.1039/b9nr00131j.

[76] Prakasam HE, Varghese OK, Paulose M, Mor GK, Grimes CA. Synthesis and photoelectrochemical properties of nanoporous iron (III) oxide by potentiostatic anodization. Nanotechnology. 2006; 17(17):4285. https://doi.org/10.1088/0957-4484/17/17/001.

[77] Norlin A, Pan J, Leygraf C. Fabrication of porous Nb_2O_5 by plasma electrolysis anodization and electrochemical characterization of the oxide. J Electrochem Soc. 2006;153(7):B225. https://doi.org/10.1149/1.2196788.

[78] Mozalev A, Bendova M, Gispert-Guirado F, Llobet E. Hafnium-oxide 3-D nanofilms via the anodizing of Al/Hf metal layers. Chem Mat. 2018;30(8):2694. https://doi.org/10.1021/acs.chemmater.8b00188.

[79] Mazierski P, Nischk M, Golkowska M, Lisowski W, Gazda M, Winiarski MJ, Klimczuk T, Zaleska-Medynska A. Photocatalytic activity of nitrogen doped TiO_2 nanotubes prepared by anodic oxidation: the effect of applied voltage, anodization time and amount of nitrogen dopant. Appl Catal B-Environ. 2016; 196:77. https://doi.org/10.1016/j.apcatb.2016.05.006.

[80] Li YM, Young L. Niobium anodic oxide films: effect of incorporated electrolyte species on DC and AC ionic current. J Electrochem Soc. 2000;147(4):1344. https://doi.org/10.1149/1.1393360.

[81] Li X, Li CY, Gong TL, Su JH, Zhang WC, Song Y, Zhu XF. Comparative study on the anodizing process of Ti and Zr and oxide morphology. Ceram Int. 2021;47(16):23332. https://doi.org/10.1016/j.ceramint.2021.05.046.

[82] Lee K, Mazare A, Schmuki P. One-dimensional titanium dioxide nanomaterials: nanotubes. Chem Rev. 2014;114(19):9385. https://doi.org/10.1021/cr500061m.

[83] Kowalski D, Kim D, Schmuki P. TiO_2 nanotubes, nanochannels and mesosponge: self-organized formation and applications. Nano Today. 2013;8(3):235. https://doi.org/10.1016/j.nantod.2013.04.010.

[84] Li PZ, Qin LY, Chen BY, Zhang SY, Zhu YX, Wang B, Zhu XF. The role of fluoride and phosphate anions in the formation of anodic titanium dioxide nanotubes. Electrochem Commun. 2024;158:107641. https://doi.org/10.1016/j.elecom.2023.107641.

[85] Zhang Y, Li PZ, Wang SY, Zhang JZ, Liu L, Liu R, Zhu XF. Effect of chloride ions on the sparking voltage of working electrolytes and its restraint method. J Phys Chem C. 2023; 127(32):16148. https://doi.org/10.1021/acs.jpcc.3c03408.

[86] Kim YD, Choi S, Kim A, Lee W. Ionic current rectification of porous anodic aluminum oxide (AAO) with a barrier oxide layer. ACS Nano. 2020;14(10):13727. https://doi.org/10.1021/acsnano.0c05954.

[87] Lin YT, Wang LK, Cheng YT, Lee CK, Tsai HE. Molecularly imprinted polymer/anodic aluminum oxide nanocomposite sensing electrode for low-concentration troponin T detection for patient monitoring applications. ACS Sens. 2021;6(6):2429. https://doi.org/10.1021/acssensors.1c00738.

[88] Ahmad H, Liu CK. Ultra-thin graphene oxide membrane deposited on highly porous anodized aluminum oxide surface for heavy metal ions preconcentration. J Hazard Mater. 2021; 415:11. https://doi.org/10.1016/j.jhazmat.2021.125661.

[89] Li YZ, Peng N, Wen YQ, Liang LB. Effect of hydrothermal treatment on porous anodic alumina generated by one-step anodization. Microporous Mesoporous Mat. 2020;306:5. https://doi.org/10.1016/j.micromeso.2020.110412.

[90] Carneiro JO, Machado F, Pereira M, Teixeira V, Costa MF, Ribeiro A, Cavaco-Paulo A, Samantilleke AP. The influence of the morphological characteristics of nanoporous anodic aluminium oxide (AAO) structures on capacitive touch sensor performance: a biological application. RSC Adv. 2018;8(65): 37254. https://doi.org/10.1039/c8ra07490a.